Rainfall Distribution in Ethiopia

Mengying Li

Columbia University

Rainfall Distribution in Ethiopia

Abstract

By utilizing GIS and R, this study addresses some topics related to rainfall distribution in Ethiopia. This paper is motivated by the payout mechanism of index insurance which aims at reducing crop losses associated with weather uncertainty in low-income agricultural economies. On the one hand, when it comes to the efficiency and inability of farmers, it is practically hard for insurance companies to confirm crop losses door to door. On the other hand, if crop is mainly affected by weather (e.g. if it suffers regularly from droughts or floods), we can base the payoff design mainly on the related climate indicators, such as spatial correlation of rainfall, to ensure that farmers affected by the same disaster get the same payoff. Rainfall is crucial for such an agriculture-fed economy as Ethiopia where geography and climate are very variable. However, different types of data, specifically, rain-gauge and satellite rainfall estimates, will yield different results. My findings suggest that elevation has a positive impact on the rainfall in most areas of Ethiopia. Rainfall has a strong clustering pattern. Different types of rainfall data will yield different results when measuring the spatial distribution of rainfall. Space-time clusters could be potentially used to validate the insurance payout complaints.

I. Introduction

Rainfall is a crucial determinant in agricultural economy as crop yield is vulnerable to spatially and temporally uneven distribution of rainfall. Index insurance, aimed at protecting farmers against climate uncertainty and encouraging banks to make loans for farmers, is developed on the basis of statistics generated from historical records of rainfall distribution. There are a lot of factors contributing to rainfall distribution patterns. Elevation is one of these

most important factors. In order to have a good knowledge of rainfall distribution, we need to figure out its relationship with these geographical features.

The economy of Ethiopia is largely driven by rain-fed agriculture. However, Ethiopia is located in the tropics and varies significantly in regional altitude (see Figure 1) , ranging from 210 m below sea level at the Denakil Depression in the northeast to over 4500 m above sea level in the Simien Mountains in the north. As shown in Figure 2, rainfall levels fluctuate significantly across time and space, which is typical of the progression of the Inter-Tropical Convergence Zone (ITCZ). The greatest concentration of rainfall happens through July to August with 366 mm as the highest monthly level. The rainfall is very scarce in the southeastern lowlands, the Ogaden Region, and the northeastern lowlands, the Danakil Desert. We can see that there is a lot of overlap between the areas with high elevation and those with high levels of rainfall. And also there seems to be a clear boundary between the rain-adequate areas and rain-scarce areas, which implies the existence of clustering pattern.

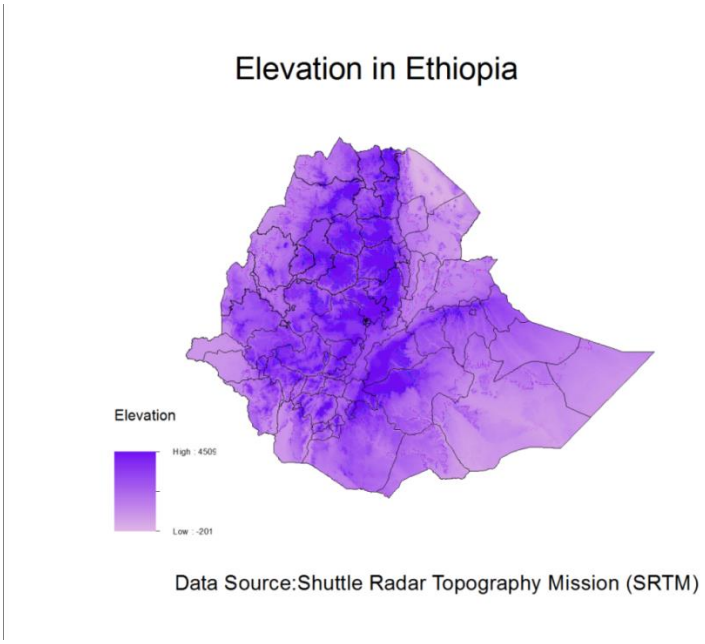

Figure 1. Elevation in Ethiopia

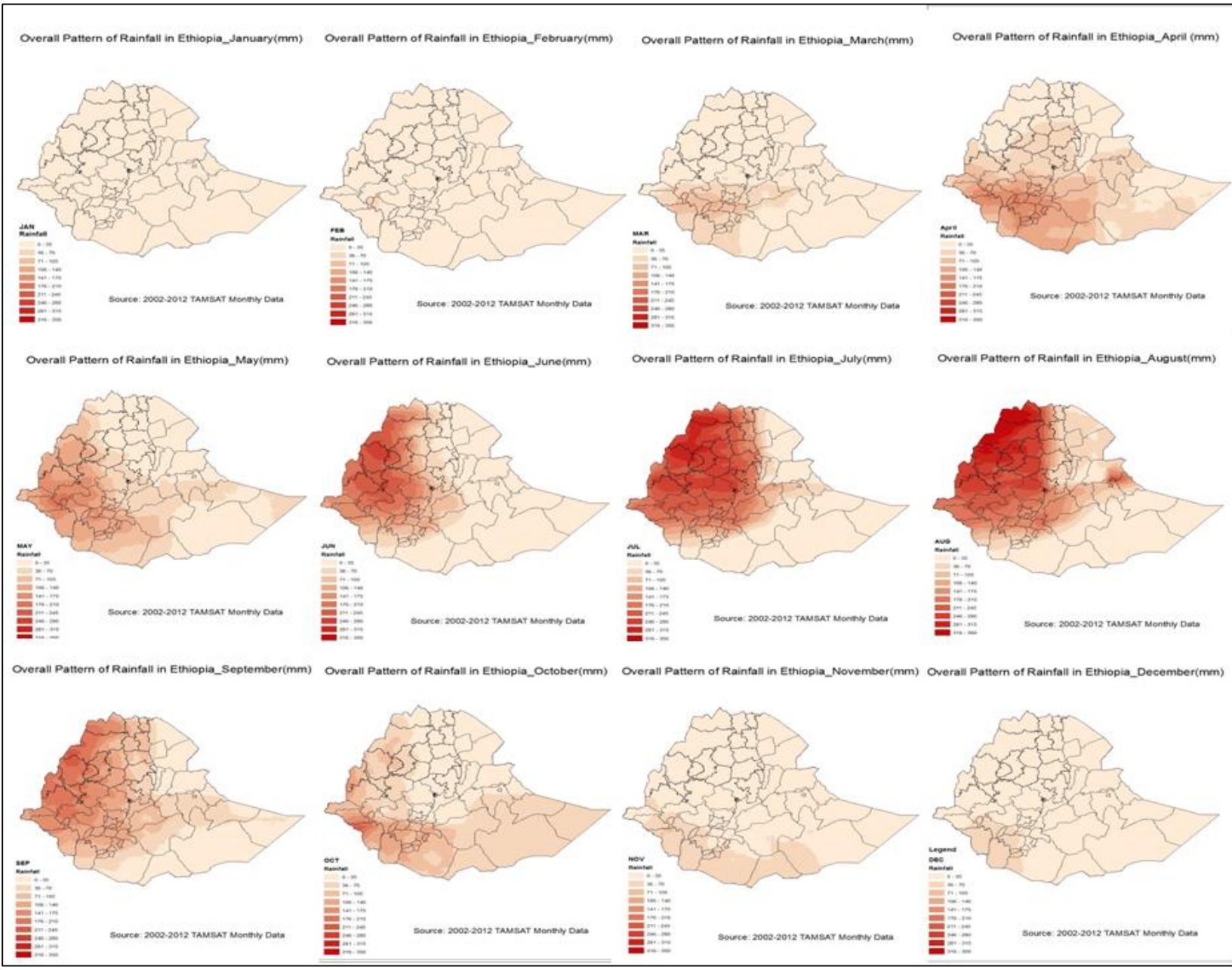

Figure 2. Monthly Rainfall Distribution

This paper is organized as follows. Following this introduction, the next section describes existing literature concerning rainfall study. The third section describes the methods used to assess the statistical properties of rainfall distribution in Ethiopia. The fourth part concludes.

II. Literature Review

There are three rainfall seasons in Ethiopia, which are known as the Kiremt, Belga,and Bega. The Kiremt season is the main rainy season and usually lasts from June to September, covering all of Ethiopia except the southern and southeastern parts (Seleshi and Zanke, 2004). The Belga season is the light rainy season and usually lasts from March to May and is the main source of rainfall for the water-scarce southern and southeastern parts of Ethiopia (Seleshi and Zanke, 2004). The Bega season is the dry season and usually lasts from October to February, during which the entire country is dry, with the exception of occasional rainfall that is received in the central sections (Seleshi and Zanke, 2004). Short cycle crops (e.g. wheat, teff, barley) that are cultivated during the Belga and Kiremt seasons constitute 5 - 10% and 40 - 45% of national crop production, respectively (Verdin et al., 2005). Long cycle crops, such as maize and sorghum, are grown during the entire Belga and Kiremt seasons and are responsible for 50% of national production (Verdin et al., 2005).

The timing, variability, and the quantity of seasonal and annual rainfall are important factors in deciding the crop yield. If precipitation is unexpectedly low in the early growing season, farmers may be able to resume production despite the loss of some of their crops (Hulme, 1990). However, if there is a rainfall break in the middle or latter growing season, all of the crops may suffer from unrecoverable damage, causing direct economic loss for farmers (Hulme, 1990).

Spatial disparity of rainfall is largely caused by elevation. A high elevation usually leads to low temperatures as the average regional temperature decreases by about 1^{o} F for every 330 ft. increase in altitude. As wet air rises, expands, and cools, it will reach its dew point (the temperature at which condensation occurs) and form a cloud. If these condensed water particles merge and become large enough they will fall as rain. According to Food and Agriculture Organization (FAO) of the United Nations (1984), rainfall in Ethiopia is generally correlated

with altitude. There are substantially more rainfall in areas with middle and higher altitudes (above 1,500 meters) than the lowlands, except the lowlands in the west where rainfall is also high. Generally average annual rainfall level of areas above 1,500 meters is larger than 900 mm.

As the same payoff of index insurance is applied to homogeneous rainfall areas, it is important to detect these regions and thereby to better understand how the payoff could be affected by the spatial and seasonal variability of precipitation climate. A lot of literature has found the existence of spatial clusters in rainfall distribution (e.g., Tu, Yan, &Wang, 2011; Matulla, Penlap, Haas, & Formayer, 2003). Local Indicators of Spatial Association (LISA) (Anselin 1995) and Moran's I scatter plots (Anselin, 1996) are among the most effective tools to evaluate climatologically homogeneous regions. The aim of LISA is to test the hypothesis of random distribution by comparing the values of one location with the values in its neighboring locations. Moran's I scatter plot visualizes the local instability in terms of a global spatial autocorrelation.

The clustering pattern of rainfall implies the existence of spatial autocorrelation of rainfall. Geostatistics tools are very common in the analysis of spatial correlation. Variogram model, for example, describes the degree of spatial dependence of a spatial random field or stochastic process. However, the variability of rainfall is also determined by the measure of timing, namely, whether it is measured in an hour, in a day or in a season. For example, heavy rains may occur at a local site, e.g., within 10^2 km^2 due to one-day local convectivity, or simultaneously over a larger area, e.g., within 10^6 km^2 in association with seasonal weather processes (Tao, 1980). In addition, as the accumulation time increases, correlation on a larger spatial scale becomes more important (Grimes, 2010). To account for the timing factor in the

variogram model, climatological variogram is therefore built up from the variograms in several time intervals, each scaled by dividing by its variance (Grimes, 2010).

Different types of rainfall data might yield different results using the same variogram model. Rain gauge data are collected from gauge stations, which give a direct picture of local rainfall levels. However, these stations are unevenly distributed and located along main roads in cities and towns, which limits the availability of rainfall data, especially in rural area where rainfall information is more important to local residents. Gauge data also suffer from the problem of gaps in the time series. Satellite proxies, particularly satellite rainfall estimate, have been used as alternatives because of their availability even over remote parts of the world. However, satellite rainfall estimates also suffer from a number of critical drawbacks, such as heterogeneous time series, short time period of observation, and poor accuracy particularly at higher temporal and spatial resolutions (Dinku, Hailemariam, Maidment, Tarnavsky and Connor, 2013). A good understanding of the difference between these two data types in the estimation of spatial distribution of rainfall will help us more precisely assess the regional rainfall homogeneity.

A lot of studies (e.g. Goovaerts, 2000) have shown that,when applied appropriately, kriging is a more accurate interpolator of rainfall than other methods. A crucial element of the kriging process is the calculation of a variogram which contains information on the variation with distance of the correlation between two points.

III. Data and Methodology

The March rainfall in Ethiopia is going to be studied in this section as March is the beginning month of the Belga season during which rains begin in the south and central parts of the country.

3.1 Data

Satellite rainfall data are from 2002-2012 TAMSAT (**T**ropical **A**pplications of **M**eteorology using **SAT**ellite) dataset. It is a feature dataset. The data is collected using 10.8 μm infra-red channel on the METEOSAT satellites and further calibrated by using a historical rain-gauge dataset of > 17,000 stations in Africa. Different types of TAMSAT products, such as decadal, monthly and seasonal data, are available. In order to compare the results generated from different types of rainfall data, daily rainfall gauge data in March of 2002 – 2006 are also introduced in this report. All the rainfall data are in millimeter.

Elevation data is from SRTM (Shuttle Radar Topography Mission) 3. It contains global coverage from 56 degrees south latitude to 60 degrees north latitude in 1 by 1 degree blocks with an approximate resolution of 90 by 90 meters. The data are in raster format and its unit is meter.

3.2 Rainfall and Elevation

In order to carry out regression analysis, the mean of elevation and rainfall level in each polygon have to be calculated first. I used zonal statistics tool in ArcMap to calculate the mean of elevation for each polygon in Ethiopia based on values from SRTM3 raster. As zonal statistics tool can be only applied for raster data but the rainfall is a feature dataset, I first used the conversion tool in ArcMap to convert it into a raster and then calculated the mean of March rainfall in each polygon and merge these two datasets together into a feature dataset.

The statistical summary of dependent variable, rainfall, and independent variable, elevation, is shown in Table 1. They are both regional average in each polygon.

Variable	Mean	Standard Deviation	Minimum	Maximum	Number of Observations
Rainfall (mm)	30.834	26.345	0	98.636	72
Elevation (m)	1600.95	577.557	388.881	2580.28	72

Table 1. Descriptive Statistics of Rainfall and Elevation

I start with a simple OLS model to quantify their relationship. The regression result is shown in Table 2. Disappointingly, the coefficient of elevation is not statistically significant and R-squared is only 0.021, which implies the misspecification of the model.

Moran's I (Moran 1950) statistics measures global spatial autocorrelation. Given a set of locations and a corresponding variable, it evaluates whether the pattern in terms of that variable is clustered, dispersed, or random. It is in the form of

$$I = \frac{n}{S_0} \frac{\sum_i \sum_j w_{ij}(x_i - \bar{x})(x_j - \bar{x})}{\sum_i (x_i - \bar{x})^2},$$

where $\bar{x}$ is the mean of the x variable, w_{ij} are the elements of the weight matrix, and S_0 is the sum of the elements of the weight matrix $S_0 = \sum_i \sum_j w_{ij}$. In the presence of spatial correlation, the absolute value of Moran's I is close to 1.

In Table 3, we can see that the Moran's I statistic is 0.8032 which is very close to 1 and highly significant, suggesting the existence of spatial autocorrelation in the model. While Moran's I statistic has great power in detecting misspecifications in the model, it is less helpful when it comes to the selection of a more appropriate model. The statistics generated from Lagrange Multiplier test can be used to indicate a better model. We can see that the robust version of Lagrange Multiplier statistics for the error model is more significant than the lag model. So the spatial error model is used here and the result is shown in Table 4.

Variable	Coefficient	Std.Error	t-Statistic	Probability
Elevation	0.0066	0.0054	1.2300	0.22280
Constant	20.212*	9.1802	2.2017	0.03098
R-squared	0.021157			

Note: *p < .05. **p < .01.

Table 2. OLS Regression

Test	MI/DF	Value	P-Value
Moran's I (error)	0.8032	10.9886	0.0000
Lagrange Multiplier (lag)	1	101.6046	0.0000
Robust LM (lag)	1	1.036	0.3087
Lagrange Multiplier (error)	1	104.3964	0.0000
Robust LM (error)	1	3.8278	0.0504
Lagrange Multiplier (SARMA)	1	105.4324	0.0000

Table 3. Spatial Autocorrelation Test

Variable	Coefficient	Std.Error	z-value	Probability
Elevation	0.01032**	0.002570	4.01482	0.0000595
Intercept	4.2011	41.8099	0.1005	0.9200
Lambda	0.9768**	0.01474	66.2746	0.0000
R-squared	0.9037			

Note: *p < .05. **p < .01.

Table 4. Spatial Error Model

In the spatial error model, a coefficient on the spatially correlated errors (LAMBDA) is added as an additional indicator and it is highly significant. The independent variable, elevation, also becomes statistically significant. The coefficient shows that one meter increase in elevation increases rainfall level by 0.01032mm on average. As a result, the fitness of the model is improved, as indicated in a higher value of R-squared.

Geographically Weighted Regression (GWR) is further used to examine how spatially consistent (stationary) the relationship between the rainfall level and elevation is across the study area. The GWR result is shown in Table 5. We can see that the number of neighbors used for local estimation is 17, which is dependent on the spatial density of rainfall and elevation. R-squared is very high: 94.04% of rainfall variance is accounted for by the regression model. Figure 3 visualizes the local relationship between elevation and rainfall level. By examining the coefficient distribution, we can see where and how much variation is present. Though rainfall increases with elevation in most parts of the country, there are also parts of the country where rainfall decreases with elevation (blue shades in Figure 3). The negative relationship is mainly distributed in the center of Ethiopia, where the altitude is also very high. This counterintuitive result is mainly due to moisture depletion as most of the moisture fall out as rain before reaching the top of the mountains (Dinku, Chidzambwa, Ceccato &Connor, 2008). However, the distribution of the relationship between elevation and rainfall is a little bit different from the finding of Dinku et al. (2008) (See Figure 4). In their paper, the most negative relationship is shown to be in the northern and southern mountainous regions.

Neighbors	17
ResidualSquares	2978.17
EffectiveNumber	25.2912
Sigma	7.985
AICc	531.546
R^2	0.9404
R^2Adjusted	0.9094

Table 5 GWR Result

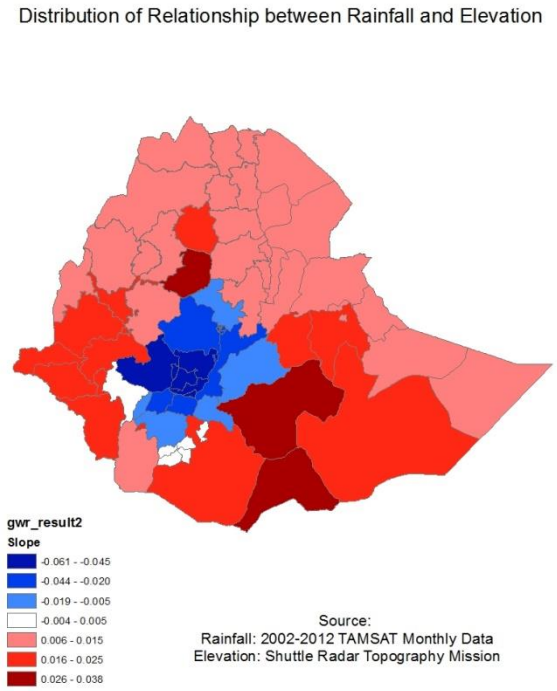

Figure 3. Distribution of Relationship between Rainfall and Elevation

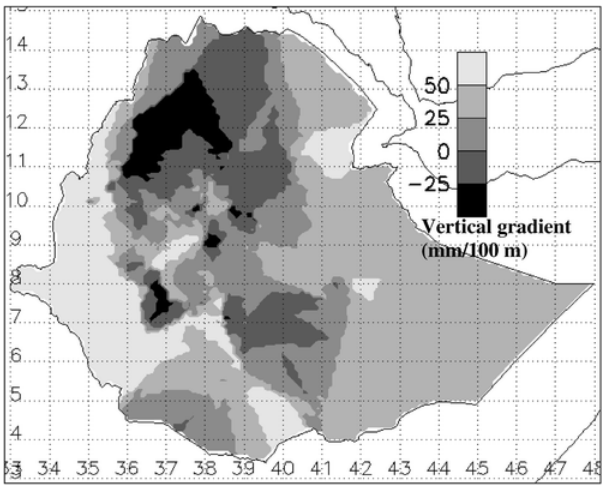

Figure 4. Variation of Mean Annual Rainfall with Elevation

Source: Dinku, et al. (2008), p.4101.

3.3 Cluster of Rainfall

The diagnostic of spatial autocorrelation in the elevation analysis has shown that neighboring rainfall exerts an effect on the rainfall itself through the error correlation. By visualizing the LISA indicator, this clustering pattern of rainfall is shown in Figure 5. The locations with significant local Moran statistics are shown in different colors based on the type of spatial autocorrelation: red is for high-high and blue is for low-low. The high-high cluster is in the southwest of Ethiopia and the north and east are low-low clusters.

The corresponding global Moran's I statistic is 0.7862 and is very significant at 99.99% level, which indicates a very strong spatial autocorrelation. However, it cannot discriminate between a spatial clustering of high values and a spatial clustering of low values in the case of a global positive spatial autocorrelation. So the scatter plot is used to specify different kinds of autocorrelation (see Figure 6). The four different quadrants of the scatterplot correspond to the four types of local spatial association between a region and its neighbors: HH, a region with a high value surrounded by regions with high values (Quadrant I in top on the right); LH, a region with low value surrounded by regions with high values (Quadrant II in top on the left); LL, a region with a low value surrounded by regions with low values (Quadrant III in bottom on the left); HL, a region with a high value surrounded by regions with low values (Quadrant IV in bottom on the right). We can see that most of the points are in the Quadrant I and Quadrant III, which is consistent with the positive Moran's I statistics. Notably, there are more observations with low-low clustering pattern than those with high-high clustering pattern.

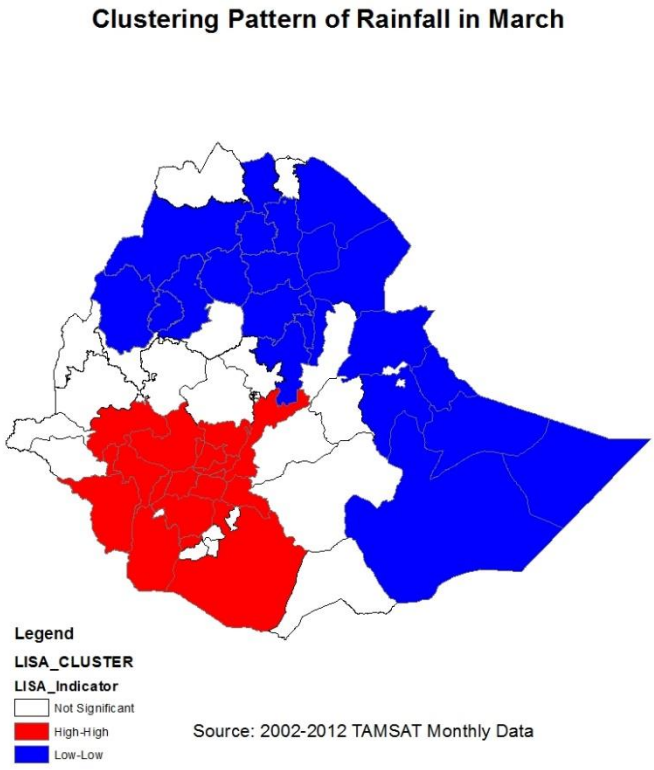

Figure 5. LISA Cluster Map of March Rainfall in Ethiopia

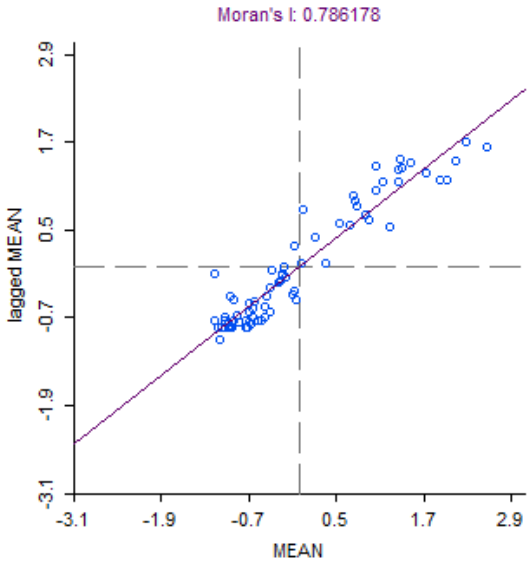

Figure 6. Moran's I Scatter Plot

3.4 Variogram and Climatological Variogram

The use of variogram is based on the concept that at a location, x, a dataset Z, can be modeled as a slowly varying mean background, m, plus a random fluctuation, R

$$Z\ \mathbf{x}=m\ \mathbf{x}+R\ \mathbf{x}$$

We now have a set of observations of Z, which in this case is rainfall level. For each pair of points within this set, the distance between them can be recorded. Now for a given distance, h, there are n subsets containing the pairs h apart (Goovaerts, 1997). The spatial dependence of the subset can then be determined by calculating the variance of the difference between each pair. After weighted by the number of pairs in each subset, the variogram is shown as below,

$$\gamma\ \mathbf{h} = \frac{1}{n\boldsymbol{h}}\sum_{i}^{n\boldsymbol{h}}(Zx_i - Zx_i + \boldsymbol{h})$$

For the statistical purpose, semivariogram is used in the paper, which is

$$\gamma^{*}\mathbf{h} = \frac{1}{2n\boldsymbol{h}}\sum_{i}^{n\boldsymbol{h}}(Zx_i - Zx_i + \boldsymbol{h})$$

The effect of rainfall is sensitive to the timing and specific event. The climatological variogram is then calculated based on the assumption that the spatial correlation of rainfall remains constant for a given region and time-period. The formula is shown as below, where k refers to k time period and the previous semivariogram will be weighted by the variance of each time period σ_k^2,

$$\gamma_c^{*}\mathbf{h} = \frac{1}{K}\sum_{i=1}^{K}\frac{1}{\sigma_k^2}\frac{1}{2n\boldsymbol{h}}\sum_{i}^{n\boldsymbol{h}}(Zx_i - Zx_i + \boldsymbol{h})$$

In this case, I am going to calculate the climatological variograms for both rain-gauge and satellite data and compare the different results in terms of their relationship to the actual rainfall intensity.

3.4.1 Gauge Data Result

The gauge stations in Oromiya area will be studied in this section. The location of gauge stations is shown in Figure 7. In order to capture the detailed information as much as possible, a 2km distance lag is chosen for nonzero data. From Figure 8, we can see the number of pairs at each binsize. For example, the first point is the number of pairs that in the first bin and the second point is the number of pairs in the second bin. After 200km, the number of pairs in each bin decreases as the distance increases. Based on Akaike Information Criterion (AIC) statistics, the double spherical model is chosen over others (see Figure 9). The nugget is about 0.4. The range is about 80 km, which implies when the distance exceeds 80 km, the spatial correlation between different locations becomes weak. Notably, though the semivariance increases with the distances, the change rate is not constant, with a turning point at about 15 km. There is more noise at the end of the actual line as less data are available in each bin at a large distance.

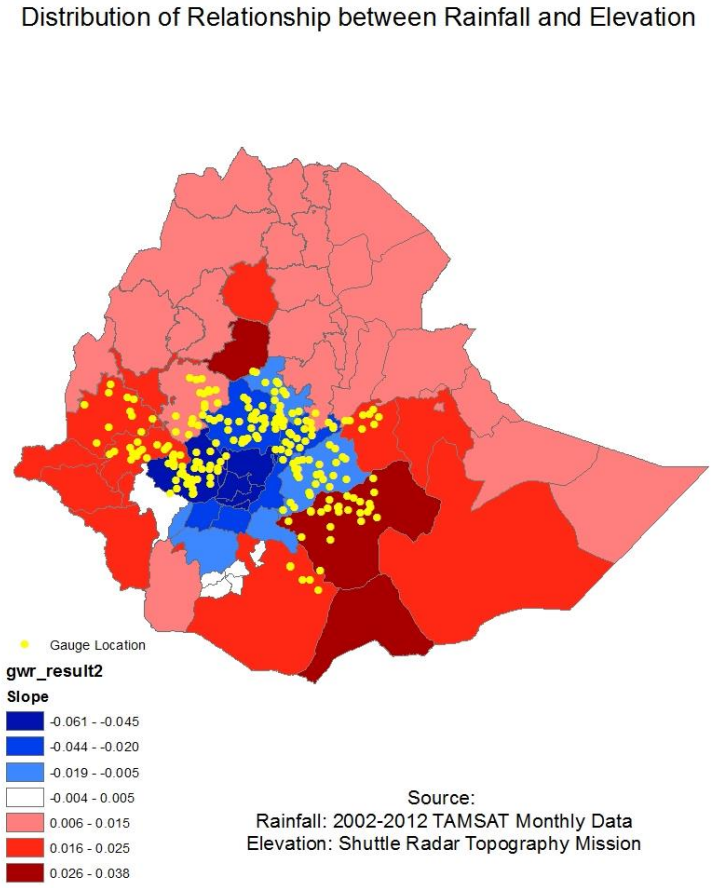

Figure 7. Location of Gauge Station in Oromiya

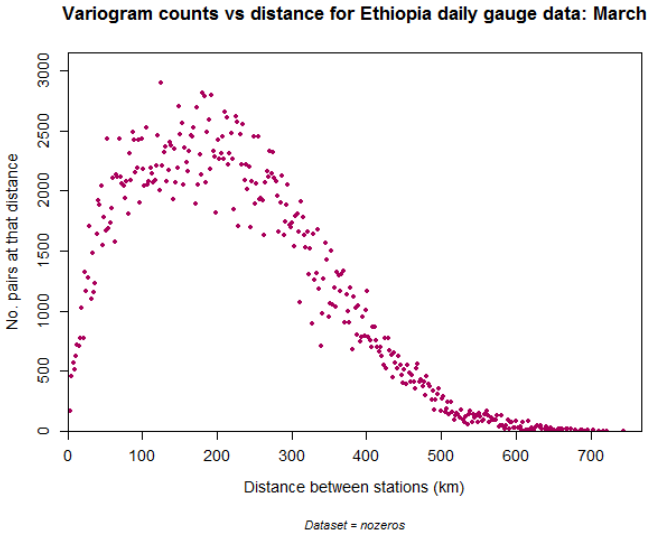

Figure 8. Number of Location Pairs in each Bin (Binsize=2km)

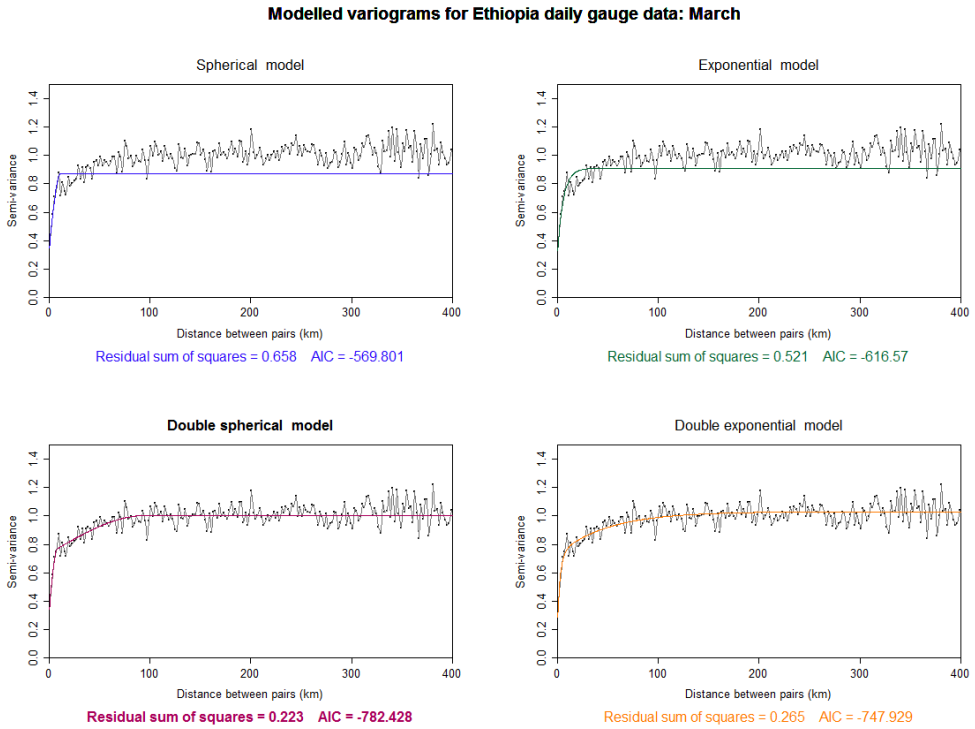

Figure 9. Different Models of Daily Gauge Non-zero Data (Binsize=2 km)

3.4.2 Satellite Result

TAMSAT satellite estimates for the same locations as the gauges are analyzed in this section. Using the same binsize as in the gauge case, we can see a large gap between these two results. According to AIC, double spherical model best describes the variance in the data (see Figure 11). Similarly, the relationship between the semivariogram and the distance is nonlinear before it reaches the sill level, however, the turning point is almost 100km and the range is almost 200 km. The result implies that remote technique seems to magnify the magnitude of rainfall correlation.

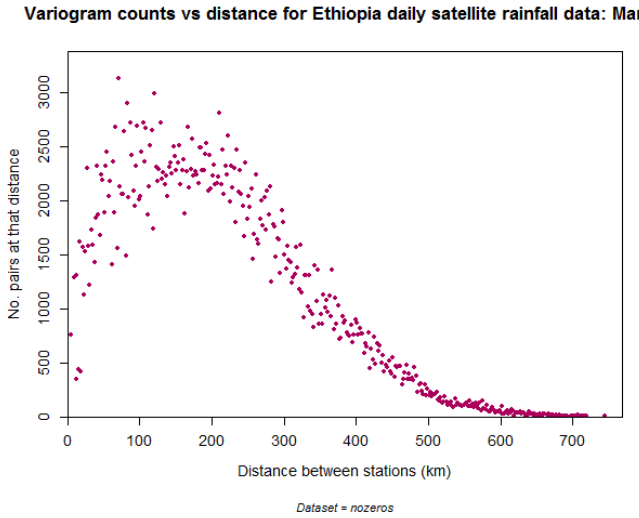

Figure 10. Number of Location Pairs in each Bin (Binsize=2 km)

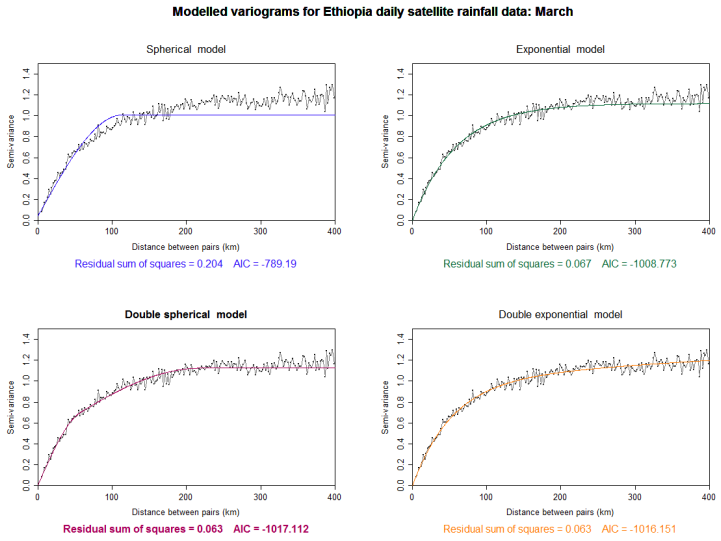

Figure 11. Different Models of Daily Satellite Data (Binsize=2)

We can visually compare the range calculated from variogram and the actual rainfall distribution in Figure 12. We can see most of rainfall patches, the ones with the same levels of rainfall are within 100 km.

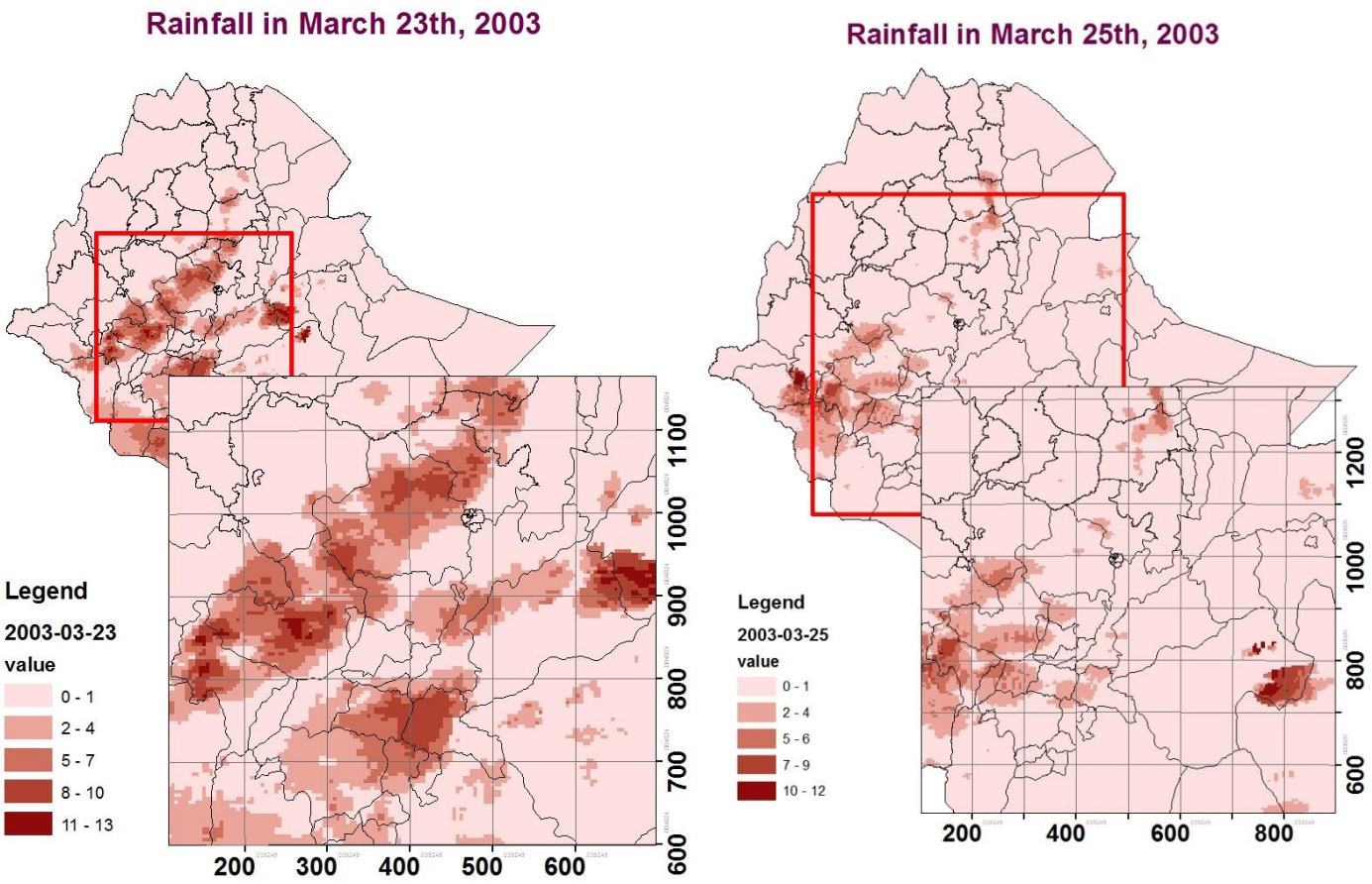

Figure 12. The Scale of Actual Rainfall Patch

The reasons for the large gap between satellite and gauge estimates are complicated. Most important one is the different mechanism of the measurement of gauges and satellites. Gauges measure rainfall directly. However, the measurement always happens at a specific time and only covers a small area. It also suffers from various problems, such as a poor spatial sampling over unpopulated areas, temporal inhomogeneity in historical records, and uncertainty associated with undercatchment[1] due to the interaction with wind and evaporation (Chen, Xie,

[1] Undercatchment by rain gages has been observed and studied since 1850. For instance, Symons (1866, 1880) reported that a 6-meter elevated rain gage caught approximately 85% of the rainfall amount received on the ground, and a rain gage installed on a church roof top of 45 meters above the ground experienced as much as a 50% undercatch.

Janowiak, & Arkin, 2002). All these problems might lead to an underestimate of the actual rainfall level and the variogram range within which rainfall are correlated. Satellite estimates look at each pixel of the target area and are based on the movement of clouds over time, which enable them to estimate rainfall levels in a wider area of and capture the dynamic change in the structure of convective rainstorms. Satellites use the height of cloud top information as indicative of rainfall; namely, they classify one area as rainy if the height of the cloud top is above a certain threshold. However, it might give us the wrong information. For example, if one area is not raining but the cloud top is high enough to reach the threshold, the satellite might mistake the non-rainy area as rainy (see Figure 13). There are also two other possible explanations related to the physical properties of the air masses as suggested by McCollum, Arnold and Mamoudou (1999), which might lead to the overestimation in satellite data. One is that the possible existence of aerosols in Africa leads to an abundance of cloud condensation nuclei, small drops, and inefficient rain processes. The other is that "convective clouds forming under dry conditions generally have cloud bases considerably higher than those of clouds forming in moist environments. This leads to an increase in the evaporation rate of the falling rain, resulting in less precipitation reaching the ground." (McCollum, et al., 1999, p666). This overestimation might imply a larger continuous surface of rainfall even the spatial autocorrelation is not that strong, which will yield a large variogram range.

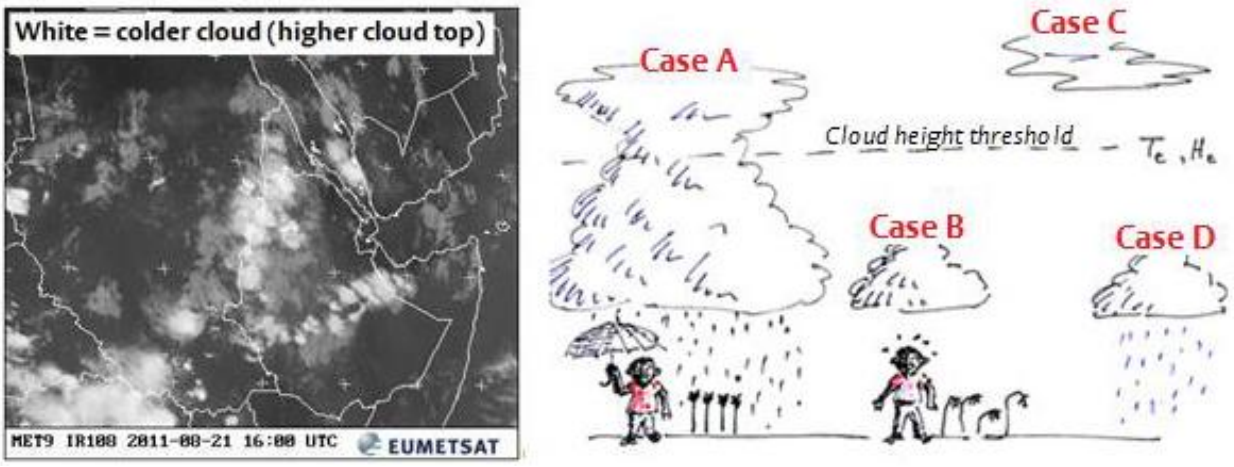

Figure 13. The Mechanism of TAMSAT Methodology

Note: *Left*: METEOSAT image of East Africa using the 10.8μm channel. The whiter the image, the colder the cloud.

Right: Schematic TAMSAT methodology.

Source: H.L. Greatrex; "Satellite rainfall information in Africa"; Statistical Services Centre, University of Reading, UK; Edition 1; 2012: P. 24

3.5 Kriging

Rainfall data are point data. It might be more in our interest to see the distribution of rainfall over a surface, which will help us detect the possible pattern of rainfall, such as cluster or trend.

Kriging, a geostatistical method to interpolate data in unsampled areas based on the climatological variogram calculated from Section 3.4, will be discussed here.

Compared with traditional interpolation approaches, such as Inverse Distance Weighted (IDW) interpolation, Kriging uses weights from semi-variogram rather than applying an arbitrary or less precise weighting scheme. As Kriging associates some probability with each prediction, hence it provides not just a surface, but some measure of the accuracy of that surface, which is known as Kriging error. The kriging process could be written in:

$$Z^*\boldsymbol{h} - m\boldsymbol{h} = \sum_{\alpha=1}^{n} \lambda_\alpha \left| Z\boldsymbol{h}_\alpha - m\boldsymbol{h}_\alpha \right|$$

Here, $\boldsymbol{h}$ and $\boldsymbol{h}_{\alpha}$ are vectors containing location information for estimation point and the neighboring data points (indexed by α). Z($\boldsymbol{h}$) is treated as a random field, with a trend m(u), and a residual component, R($\boldsymbol{h}$) = Z($\boldsymbol{h}$) - m($\boldsymbol{h}$). Kriging estimates the residual at h as a weighted sum of the residuals at n surrounding data points. Kriging weights at each surrounding point, λα, are derived from the semi-variogram (Bohling, 2005). This equation can then be used to give a final estimate of Z($\boldsymbol{h}$) by minimizing the variance of the estimator in a process described in detail in Goovaerts (1997). If a climatological variogram has been used, the final kriging variance must also be re-scaled by multiplying the result from each event by its variance.

3.5.1 Simple Kriging

Simple kriging assumes that the trend component is a constant over the entire domain i.e. $m\boldsymbol{h} = m$. Kriging with external drift, or universal kriging, caters for datasets which have an underlying trend in the mean.

So far, all of these methods currently. It is computationally expensive to estimate Z over many unsampled points and take an average if one wishes to know the value of Z at a pixel. Instead, the process of block kriging can be used. This simply applies the kriging methodology described above to find the average expected value in an area around an un-sampled point, rather than the value at the point itself.

Here I used the rainfall data on three dates, specifically, March 15th, 2002, March 30th, 2004 and March 13th, 2005, as demos to show the simple kriging results. Two data types, i.e. raw data and indicator rain gauge data (1 is for rainfall, 0 is for no rainfall) were used on each day. The sample kriging results can be seen fromTable 6. The semivariograms generated from indicator data can be shown in Figure 14. The interpolation from indicator data gives the rainy probability of each location, ranging from 0 to 1. We can see that the unsampled points close to the known location have a similar value associated with them.

However, we can see that the ordinary kriging method suffers from several problems. As the kriged value is mean-based, which implies that even an unsampled point is far away from the input data, it will still be assigned a value as the mean. That's why some areas seem to be close to the no-rain locations and supposedly to be dry, or distant from the sampling areas, still have non-zero values.

PointID	Longitude	Latitude	Estimate1	Error1	Estimate2	Error2	Nearest (km)
…	…	…	…	…	…	…	…
A12911	39.144	7.019	11.35	5.35	2.07	0.67	28.3
A12912	39.181	7.019	11.35	5.35	2.12	0.67	24.1
A12913	39.219	7.019	11.34	5.34	2.17	0.66	20
A12914	39.256	7.019	11.31	5.34	2.22	0.65	15.9
A12915	39.294	7.019	11.26	5.32	2.27	0.63	11.7
A12916	39.331	7.019	11.16	5.26	2.32	0.6	7.6
A12917	39.369	7.019	11	5.11	2.38	0.58	3.5
A12918	39.406	7.019	10.81	4.86	2.42	0.55	0.7
A12919	39.444	7.019	10.92	5.03	2.44	0.56	4.8
A12920	39.481	7.019	11.1	5.23	2.46	0.58	9
A12921	39.519	7.019	11.22	5.31	2.47	0.6	13.1
A12922	39.556	7.019	11.29	5.33	2.48	0.61	17.2
A12923	39.594	7.019	11.32	5.34	2.49	0.62	21.1
A12924	39.631	7.019	11.34	5.35	2.51	0.62	17.5
A12925	39.669	7.019	11.34	5.35	2.52	0.61	14.1
A12926	39.706	7.019	11.35	5.35	2.54	0.59	11.3
A12927	39.744	7.019	11.35	5.35	2.57	0.56	9.4
A12928	39.781	7.019	11.35	5.35	2.59	0.55	9.2
A12929	39.819	7.019	11.35	5.35	2.6	0.55	10.7
A12930	39.856	7.019	11.35	5.35	2.62	0.55	13.4
…	…	…	…	…	…	…	…

Table 6. Kriging Result Sample (March 15th, 2002)

Note: Estimate1 and error1 are from the kriging using raw data.
Estimate2 and error2 are from the kriging using indicator data.
Nearest means the nearest point from the kriged one.

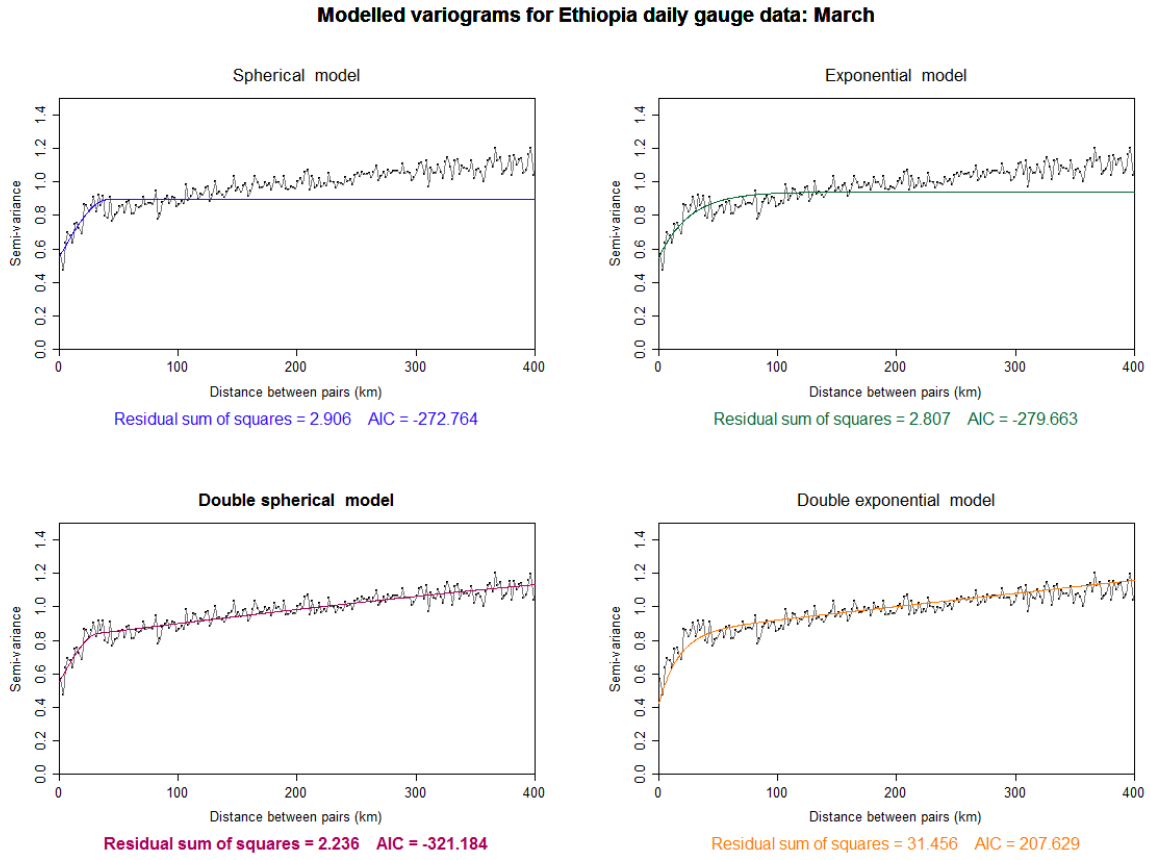

Figure 14. Different Models of Daily Satellite Indicator Rainy Data (Binsize=2)

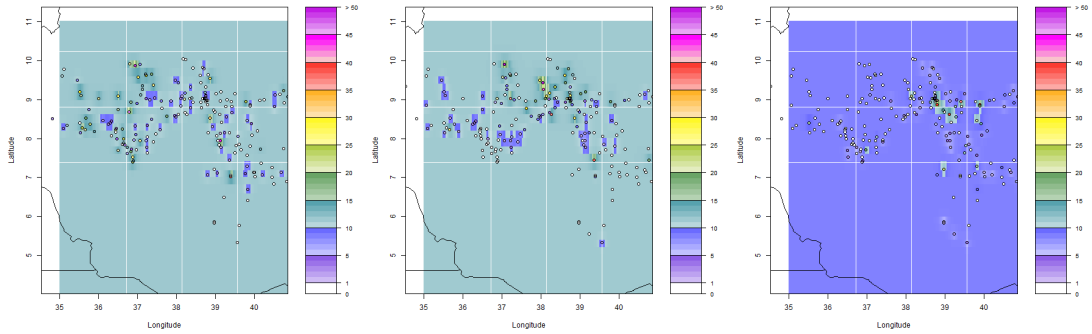

March 15th, 2002 March 30th, 2004 March 13th, 2005

Figure 15. Kriged Daily Rainfall for Oromiya (Raw Data)

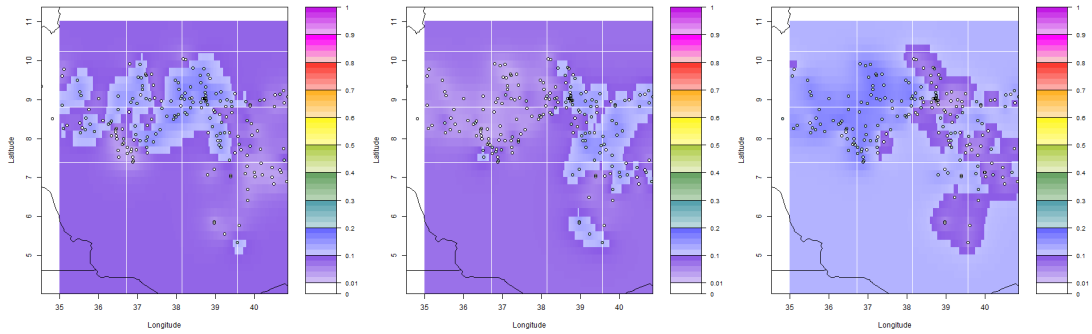

March 15th, 2002 March 30th, 2004 March 13th, 2005

Figure 16. Kriged Daily Rainfall for Oromiya (Indicator Data)

3.5.2 Double kriging

It might be expected that the spatial correlation associated with rainfall occurrence will be different to the one associated with rainfall amount. In addition, as rainfall is a positive quantity, estimated rainfall values at an unsampled location will never equal zero and will approach the mean of the observations when estimating at large distances from a gauge. This is not ideal if it is important to accurately capture rainfall occurrence. The issue can be addressed through the approach of Barancourt et al. (1992), who suggested that rainfall at a location i can be seen as the product of amount, F and occurrence, I, which can be calculated individually from the dataset

$$Z_i = I_i F_i$$

Rainfall occurrence is calculated through the use of indicator kriging, where the data at each pixel and day has been converted into a binary value (1 if rainy and 0 if dry).

The result of the process is a kriged map of the probability of rainfall. A threshold probability can then be selected in order to convert the probability map into a rain/no rain mask. In this paper, the threshold for each day was selected as equivalent to the proportion of gauges which recorded rain on that day. Rainfall amount is then derived by applying the variogram/kriging process to just the observed positive rainfall amount i.e. ignoring zero-rainfall values in the observations. This also has the advantage of making the observed distribution more Gaussian and a normal scores transformation is rarely needed in this case (Greatrex, 2010).

The double kriged daily rainfall on these three days can be shown in Figure 17. We can see that different from previous purely raw data and indicator kriging maps, these double-kriged maps have the zero rainfall areas, which makes more sense.

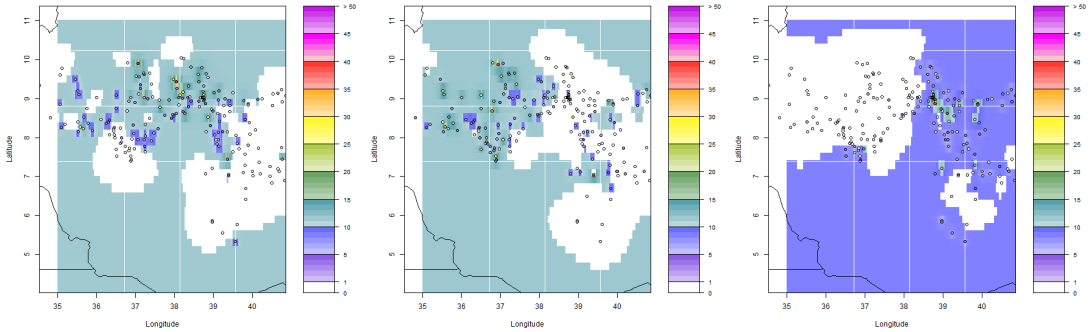

March 15th, 2002 March 30th, 2004 March 13th, 2005

Figure 17. Double Kriged Daily Rainfall for Oromiya

IV. Further Development: Space-Time Cluster

Now, there are a lot of index insurance projects where stakeholders are asking to focus on pixels over tens of thousands of sites (e.g Burkina), so it might make sense to start looking at regional indices. Most complaints are from villages that neighboring villages got a different payout from them but in fact they had the "same" year. Also, big events normally pay out over large regions.

In order to specify the boundary of each “similar” area, I used SatScan for monthly rainfall occurrence data from 1983-2013 in Tigray area in Ethiopia in an attempt to figure out the possible space-time clusters. Figure 18-20 show the space-time clusters for June, August and seasonal (June-September) rainfall occurrence. We can see that the “blue” and “red” clusters are the most stable ones but the yellow and pink ones seem to be more sensitive to different time dimensions. More interestingly, the north area of Tigray has a “non-clustering” cluster and it turns out these areas are the ones with the strongest complaint about their payout they got from the index insurance. It might be because that these areas don’t have a regular pattern in terms of rainfall and their expectation from the index insurance might be biased.

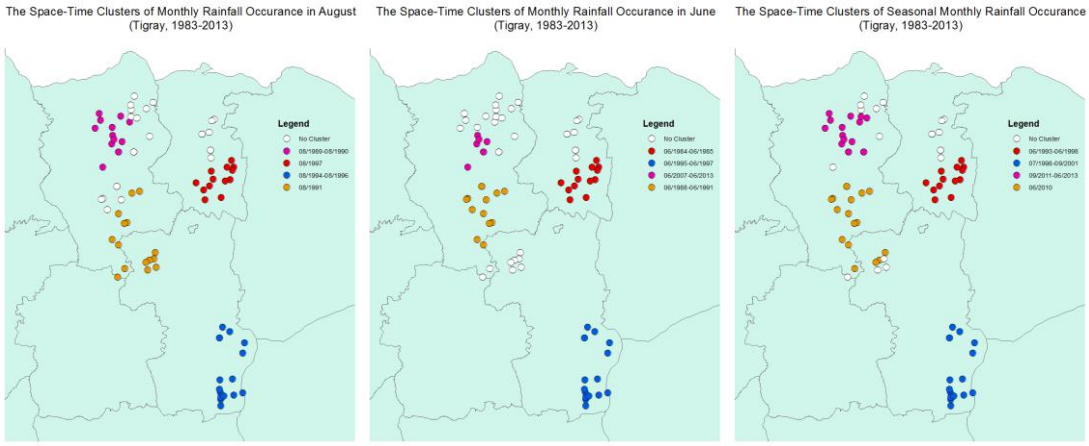

Figure 18. Space-time Clusters for Rainfall Occurrence in Tigray (1983-2013)

V. Conclusion

This paper provides a framework of rainfall distribution in Ethiopia. A generally positive relationship between rainfall and elevation has been found. However, the relationship does not hold constant if we look at it locally; some parts might exhibit a negative impact of elevation on rainfall. This inconsistency in rainfall-elevation relationship confirms the finding of Dinku (2008). The estimates for the range of rainfall correlation using satellite data are more than twice as large as them generated from gauge data. As index insurance is designed in such a way that farmers in the areas where rainfall is spatially correlated will get the same payoff, a smaller number of farmers are expected to get the payoff in face of the losses caused by rainfall if we calculate the rainfall correlation on the basis of gauge data and a larger number getting the payoff if the calculation is based on satellite data. Further work should be done in how to combine these two estimates, i.e., gauge estimates and satellite estimates, to have a better estimate of rainfall correlation and thereby to generate a more reasonable payoff for farmers.

This paper introduces different kriging methods using different types of data. We can see that double kriging method yields a more reasonable result than ordinary kriging.

Besides the traditional clustering method, this paper further addresses the potential use of space-time clusters to detect the areas which are suitable for collective purchase of the same type of index insurance.

VI. References:

Bohling, G. (2005), Kriging, in *Course notes for Data Analysis in Engineering and Natural Science*, edited, Kansas Geological Survey, Kansas.

Chen, M., Xie, P., Janowiak, J. E., & Arkin, P. A. (2002). Global land precipitation: A 50-yr monthly analysis based on gauge observations. *Journal of Hydrometeorology*, 3(3), 249-266.

Cheung, W. H., Senay, G. B., & Singh, A. (2008). Trends and spatial distribution of annual and seasonal rainfall in Ethiopia. *International journal of climatology*, 28(13), 1723-1734.

Dinku, T., Chidzambwa, S., Ceccato, P., Connor, S. J., & Ropelewski, C. F. (2008). Validation of high‐resolution satellite rainfall products over complex terrain. *International Journal of Remote Sensing*, 29(14), 4097-4110.

Dinku, T., Hailemariam, K., Maidment, R., Tarnavsky, E., & Connor, S. (2013). Combined use of satellite estimates and rain gauge observations to generate high‐quality historical rainfall time series over Ethiopia. *International Journal of Climatology*.

Food and Agriculture Organization of the United Nations (1984). *Agroclimatic Resource Inventory for Land use Planning*. Ethiopia. Technical Report 2. AG: DP/ETH/78/003, Rome.

Greatrex, H., 2010. The application of seasonal rainfall forecasts and satellite rainfall observations to crop yield forecasting for Africa. PhD thesis, University of Reading.

Grimes, D. I., & Pardo‐Igúzquiza, E. (2010). Geostatistical analysis of rainfall. *Geographical Analysis*, 42(2), 136-160.

Goovaerts, P. (1997). Geostatistics for natural resources evaluation. Oxford university press.

Hulme, M. (1992). Rainfall changes in Africa: 1931–1960 to 1961–1990. *International Journal of Climatology*, 12(7), 685-699.

Matulla, C., Penlap, E. K., Haas, P., & Formayer, H. (2003). Comparative analysis of spatial and seasonal variability: Austrian precipitation during the 20th century. *International Journal of Climatology*, 23(13), 1577-1588.

McCollum, Jeffrey R., Arnold, Gruber & Mamoudou, B. Ba (1999).Discrepancy between Gauges and Satellite Estimates of Rainfall in Equatorial Africa. J. Appl. Meteor., 39, 666–679.

Moran, P. A. (1950). Notes on continuous stochastic phenomena. Biometrika, 37(1/2), 17-23.

Seleshi, Y., & Zanke, U. (2004). Recent changes in rainfall and rainy days in Ethiopia. *International Journal of Climatology*, 24(8), 973-983.

Tao, S. (1980). Torrential Rain in China, Science Press, Beijing, 31–33.

Tu, K., Yan, Z. W., & Wang, Y. (2011). A spatial cluster analysis of heavy rains in China. Atmos. *Oceanic Sci. Lett*, 4, 36-40.

University of Arizona School of Natural Resources and the Environment (2011). Elevation, elevation, elevation. *The Rimrock Report*, 4(2) .

Verdin, J., Funk, C., Senay, G., & Choularton, R. (2005). Climate science and famine early warning. *Philosophical Transactions of the Royal Society B: Biological Sciences*, 360(1463), 2155-2168